Accepted Manuscript

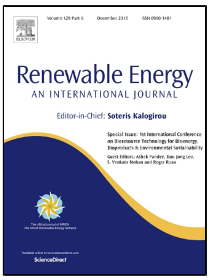

An overview of ultra-refractory ceramics for thermodynamic solar energy generation at high temperature

Laura Silvestroni, Diletta Sciti, Luca Zoli, Andrea Balbo, Federica Zanotto, Roberto Orrù, Roberta Licheri, Clara Musa, Luca Mercatelli, Elisa Sani

PII:	S0960-1481(18)30986-8
DOI:	10.1016/j.renene.2018.08.036
Reference:	RENE 10463
To appear in:	*Renewable Energy*
Received Date:	21 March 2018
Accepted Date:	09 August 2018

Please cite this article as: Laura Silvestroni, Diletta Sciti, Luca Zoli, Andrea Balbo, Federica Zanotto, Roberto Orrù, Roberta Licheri, Clara Musa, Luca Mercatelli, Elisa Sani, An overview of ultra-refractory ceramics for thermodynamic solar energy generation at high temperature, *Renewable Energy* (2018), doi: 10.1016/j.renene.2018.08.036

An overview of ultra-refractory ceramics for thermodynamic solar energy generation at high temperature

Laura Silvestroni[1], Diletta Sciti[1*], Luca Zoli[1], Andrea Balbo[1,2], Federica Zanotto[2], Roberto Orrù[3], Roberta Licheri[3], Clara Musa[3], Luca Mercatelli[4], Elisa Sani[4]

[1]*CNR-ISTEC, Institute of Science and Technology for Ceramics, Via Granarolo 64, I-48018 Faenza (Italy);*

[2]*Corrosion and Metallurgy Study Centre "Aldo Daccò", Engineering Department, University of Ferrara, G. Saragat 1, Ferrara 44122, Italy;*

[3]*Mechanical Engineering, Chemistry and Materials Department, University of Cagliari, via Marengo 2, Cagliari 09123, Italy;*

[4]*CNR-INO, National Institute of Optics, Largo E. Fermi, 6, I-50125 Firenze, Italy;*

**corresponding author: diletta.sciti@istec.cnr.it, ISTEC-CNR, Faenza, Italy*

ABSTRACT

An efficiency improvement of concentrating solar power systems relies on a significant increase of the operating temperatures, exceeding 600°C. This goal can be achieved through the use of solar absorbers possessing high spectral selectivity and stability at such temperatures. Suitable alternatives to the largely used silicon carbide can be found in the ultra-high temperature ceramics class. This study focuses on the effect of processing, microstructure evolution and surface texture on the optical properties at room and high temperature. ZrB_2-based ceramics are taken as case study to detect any correlation amongst composition, porosity, mean grain size, roughness and spectral selectivity. In addition**,** the effect of surface variation, induced by chemical etching or by exposure to oxidizing environment, thus simulating the actual operation conditions, are evaluated and compared to SiC

optical properties. Absorbance and solar selectivity are discussed as a function of the microstructural and surface properties upon detailed roughness characterization. Advantages in the use of UHTC as solar absorbers, strength and criticalities related to the use of these ceramics in comparison with SiC are discussed.

Keywords: Ultra-High Temperature Ceramics; ZrB_2; optical properties; solar absorbers; concentrating solar power, ageing.

1. Introduction

The worldwide growing concern with environmental preservation has forced changes in energy management, promoting the pursuit of new technologies for energy production. In addition, as the world's population is expected to expand, the demand for energy will grow as well. Hence, the use of clean, safe and cost-effective energy supplies, such as solar energy, will have a fundamental role within the global social and economic framework. Concentrating Solar Power (CSP) technology is a safe, sustainable and cost-effective energy supply [1–5]. In CSP technology, the heat absorbed on the collector material is transferred to a heat transfer fluid, which plays a very vital role in determining the overall efficiency of solar energy utilization. The efficiency of solar thermal power plants indeed increases rapidly with increasing working temperatures. Currently, the typical temperatures achieved in solar towers are around 565°C when molten salts are used as heat transfer fluid, but may exceed 600°C on the tube outer surface [6]. Only in few cases, in open volumetric air receivers, direct heating of air is also being reported to achieve very high temperatures approximating 800°C [7–9]. In any case, to improve the competitiveness of this power generation technology, the receiver performance has to be improved, particularly its stability at high temperatures.

In the framework of the Italian project SUPERSOLAR (*http://www.ino.it/supersolar*), ceramic materials aimed to be used as absorbers in thermal solar energy plants operating at temperatures higher than current systems have been investigated and developed.

Diborides and carbides of zirconium, hafnium and tantalum (ZrB_2, ZrC, HfB_2, HfC, TaB_2, TaC), referred to as Ultra-High-Temperature-Ceramics (UHTCs), are considered the best-emerging materials for applications in aerospace and advanced energy systems (turbine blades, combustors, scramjet engines, nuclear fusion reactors) [10]. The increasing interest in these materials is due to their unique combination of properties, including the highest melting points of any group of materials, >3000°C, elevate strength at extreme temperature, like 600-800 MPa at 1500-2100°C [11], high thermal conductivity, 80-110 W/mK up to 2000°C [12] and chemical stability. Recently**,** it has been found that most of these compounds also have the characteristic of being intrinsic solar selective materials [13–19], but the understanding of the optical properties of these materials is still very scanty, especially at high temperature. UHTCs have thus the potential to be suited for application in high temperature solar receivers, once their basic properties have been properly investigated and correlated to the bulk and surface characteristics.

The main objective of SUPERSOLAR project was to systematically study the UHTC fundamental optical properties, i.e. light absorption and emission at room and high temperatures. Particular emphasis was devoted to identify their correlation with relevant material characteristics, such as compositions, porosity, surface finishing. Several ultra-refractory boride and carbides have been studied in the framework of the project [13–17], allowing to identify the most promising materials for solar absorber applications. This work describes, as a case study, an extensive work on ZrB_2-based ceramics, consolidated through different processes, with or without $MoSi_2$ as secondary phase, textured or with controlled porosity. Among UHTC materials, ZrB_2 was selected for broad characterization in view of a number of advantages on several aspects: borides possess better thermo-mechanical properties and higher oxidation resistance than carbides [10,20], it has lower weight than

other transition metals compounds, around 6 g/cm^3 compared to 11-12 g/cm^3 for Hf- or 11-14 g/cm^3 for Ta- based compounds, and, least but not last, ZrB_2 is the cheapest raw powder in this class.

The literature shows several reports about the mechanical property changes of ZrB_2 as a function of different processing parameters [20–24], while, to the best of our knowledge, the impact on optical properties has been not investigated yet. For the preparation of the ZrB_2-based composites, $MoSi_2$ was selected in this work as sintering additive in view of its properties compatible with the high-temperature environment, i.e. melting point above 2000°C, high stiffness [25] and owing to its beneficial effects on densification, high temperature strength and oxidation resistance improvement of borides [20,26].

The effect of microstructural and surface features is then correlated to the optical absorbance and spectral selectivity. In addition, the optical properties of these ceramics exposed to oxidizing environment, simulating the prolonged use in air at high temperature, are discussed and compared to the performances of the currently used absorber materials, mostly based on silicon carbide (SiC). Finally, high temperature spectral emittance spectra of ZrB_2 composites are shown and compared to that of SiC.

2. Materials and Methods

2.1 Materials preparation and characterization

Spark plasma sintered material. A bulk pure ZrB_2 material was prepared starting from Self propagating High-temperature Synthesized (SHS) powders and consolidated by spark plasma sintering (SPS), sample ZBM0-s, according to the procedure reported in [27]. Briefly, before being consolidated, the SHS product received a mild ball milling treatment to generate powders with an average particles size of 6.7 μm and d_{90} parameter value of 16.8±1.0 μm. The SPS process was conducted using a 515S model equipment (Fuji Electronic Industrial Co., Ltd., Kanagawa, Japan) under vacuum (20 Pa) conditions.

Hot pressed materials. ZrB_2-composites containing $MoSi_2$ were prepared using commercial raw powders: ZrB_2 (H. C. Starck, Germany. Grade B), mean particle size: 1.5 μm, impurities (wt%): C 0.25, O 2.0, N 0.25, Fe 0.1, Hf 0.2; $MoSi_2$ (Aldrich, Milwaukee, USA), mean particle size: 2.8 μm, impurities (wt%): O 1.0. The amount of sintering agent ranged from 5 to 50 vol% to enable full densification and labeled hereafter as ZBMX, where X = 5, 10, 20, 30, 50. The mixtures were prepared by wet milling for 24 h using absolute ethanol and SiC milling media, followed by drying in a rotary evaporator and sieving through 250 μm screen. 30 mm diameter green pellets were prepared by uniaxial pressing with 20 MPa. Hot pressing was performed in low vacuum (~100 Pa) using an induction-heated graphite die at temperatures between 1750 and 1900°C with an uniaxial pressure of 30 MPa during heating and a dwell at the maximum temperature set on the basis of the shrinkage curve, as reported in Table I.

Pressureless materials: ZrB_2-composites containing 20 vol% $MoSi_2$ were sintered in a graphite furnace (Astro industries Inc., Santa Barbara, USA) without applied pressure, with a heating rate of 600°C/h under flowing argon atmosphere (~0.1 MPa) at 1950°C for 60 minutes, as indicated in Table I, sample ZBM20-ps. Additionally, for high temperature emittance measurements, one 40-mm diameter pellet with 10 vol% $MoSi_2$ and with a pore-forming agent, ZBM10P, was prepared and pressureless sintered in the same graphite furnace at 1950°C reaching a relative final density of 87%.

Texture modification and ageing: Surface texture modifications were induced by chemical etching in order to improve the solar radiation absorption. In particular, the polished surface of ZBM10 samples was exposed to a mixture of mineral acid (HF/HNO_3) for few seconds, thereafter labelled as ZBMetc.

In addition, the effect of prolonged exposure to high temperatures was evaluated by oxidation of the same composition in air furnace at 800 and 1200°C for 10 hours (Nannetti1700°C, mod. FH 65/17, Faenza, Italy). The resulting oxidized surfaces were labelled as ZBM800 and ZBM1200.

For the as-sintered materials, the bulk densities were measured by Archimedes' method in distillate water according to the ASTM C373-88 standard and the microstructure was analyzed on polished or

treated surfaces by scanning electron microscopy (FE-SEM, Carl Zeiss Sigma NTS Gmbh, Oberkochen, DE) and energy dispersive x-ray spectroscopy (EDS, INCA Energy 300, Oxford instruments, UK). The optical surface of the pellets were polished by diamond paste with decreasing grain size, from 30 to 1 μm using a standard procedure. Quantitative calculations of the microstructural parameters, like residual porosity, mean grain size and secondary phase content, were carried out via image analysis with a commercial software package (Image-Pro Plus® version 7, Media Cybernetics, Silver Springs, MD, USA).

The surface texture characterization was carried out with a non-contact optical profilometer (Taylor-Hobson CCI MP, Leicester, UK) equipped with a green light and a 20X magnification objective lens. For each samples, at least two distinct areas (0.8×1 cm^2) were scanned along two orthogonal directions and the collected surface data were processed with the Talymap 6.2 software (Taylor-Hobson, Leicester, UK). The analysis of surface data was carried out in terms of areal field parameters, as 3D parameters can provide a more comprehensive information about surface texture with respect to 2D ones. The evaluation of 3D texture parameters was performed following the ISO 25178-2:2012 standard on the two datasets collected for each sample, after denoising (median filter 5×5), form removing and filtering with an aerial robust gaussian L-filter.

2.2 Methods and parameters for optical characterization

The parameters selected to qualify the materials were hemispherical reflectance, high temperature emittance and spectral selectivity.

- Hemispherical reflectance spectra were acquired using two instruments: a double-beam spectrophotometer (Perkin Elmer Lambda900) equipped with a Spectralon®-coated integration sphere for the 0.25-2.5 μm wavelength region and a Fourier Transform spectrophotometer (FT-IR Bio-Rad "Excalibur") equipped with a gold-coated integrating sphere and a liquid nitrogen-cooled detector for the range 2.5-16.5 μm.

- High temperature emittance spectra were obtained as the ratio between the radiance emitted by the sample heated in a home-made high-vacuum furnace (ultimate pressure limit few 10^{-6} mbar, maximum temperature around 1200K), and that emitted by a reference blackbody (C.I. Systems SR-2) at the same temperature. Radiances were detected and spectrally resolved by the FT-IR "Excalibur" spectrophotometer described above. Details of the experimental apparatus can be found in [28]. The available spectral range for high temperature emittance measurements was between 2 and 21 μm wavelength.
- As a third evaluation parameter, spectral selectivity was calculated as the ratio between the total solar absorbance, α, and the estimated hemispherical emittance, ε. α, is given, in terms of the experimental room-temperature hemispherical reflectance ρ∩(λ), by the following expression:

$$\alpha = \frac{\int_{\lambda_{min}}^{\lambda_{max}} (1-\rho^{\cap}(\lambda)) \cdot S(\lambda) d\lambda}{\int_{\lambda_{min}}^{\lambda_{max}} S(\lambda) d\lambda} \quad (1)$$

where S(λ) is the Sun emission spectrum [29] and the integration is carried out between λ_{min}=0.3 μm and λ_{max}=2.3 μm. The estimated hemispherical emittance, ε, at the temperature of 1200 K, taken as hypothetical working temperature of a future solar absorber, was determined as follows:

$$\varepsilon = \frac{\int_{\lambda_1}^{\lambda_2} (1-\rho^{\cap}(\lambda)) \cdot B(\lambda,1200K) d\lambda}{\int_{\lambda_1}^{\lambda_2} B(\lambda,1200K) d\lambda} \quad (2)$$

where B(λ,1200K) is the blackbody spectral radiance at 1200K temperature and the integration is carried out in the interval λ_1=0.3 μm- λ_2=16.0 μm.

3. Results

3.1 Microstructure

Polished surfaces - To correlate the optical spectra to compositional characteristics, SEM/EDS characterization was carried out on the optically investigated surfaces. All spark plasma sintered and hot pressed ceramics achieved density above 95%, Table I. Examples of the microstructures obtained are displayed in Fig. 1 a-d. The combination of the SHS method with the SPS technique allowed for the obtainment of an additive-free ZrB_2 product, ZBM0-s, with relatively high density level, Fig. 1a and Table I. The use of high mechanical pressures, 60 MPa, contributed to such achievement [27].

Label	$MoSi_2$ vol%	Sintering technique	T,t,P °C, min, MPa	Bulk relative density %	Surface porosity vol%	Mean pore size µm	Mean g.s. µm	Max g.s. µm	Min g.s. µm	Secondary phases by SEM-EDS vol%
ZBM0-s	0	SPS	1850,20,60	>96	~4	4.90	19±6	33.5	8.5	-
ZBM5	5	HP	1900,10,30	>98	~2	0.13	1.9±0.7	3.6	0.9	1.4 $MoSi_2$, 1.5 SiO_2/SiC
ZBM10	10	HP	1850,10,30	>96	~4	0.13	2.4±0.6	3.9	1.4	8.5 $MoSi_2$, 1.4 SiO_2, 0.7 SiC
ZBM20	20	HP	1800,4,30	>98	~2	0.10	2.4±0.9	5.4	0.6	13 $MoSi_2$, 2.5 SiO_2, 2.0 SiC, 0.7 $ZrO_2$2, 0.6 MoB
ZBM30	30	HP	1850,3,30	>98	~2	0.10	1.7±0.6	3.6	0.6	28.4 $MoSi_2$, 3.4 SiO_2/SiC
ZBM50	50	HP	1750,13,30	>98	~2	0.10	1.9±0.8	4.3	0.7	39 $MoSi_2$, 6.5 SiO_2, 2 MoB, 1 ZrO_2, 1 SiC
ZBM20-ps	20	PS	1950,60,-	>98	~2	1.45	2.6±0.7	1.3	4.1	18 $MoSi_2$, 2 MoB, 0.5 SiO_2
ZBM10P	10	PS	1950,60,-	~87	~13	4.70	2.8±0.7	5.2	1.2	8 $MoSi_2$, 2 MoB

Table I: Composition, sintering technique and parameters, T: maximum temperature, t: dwell at T, P: applied pressure, relative density, porosity features, mean, maximum and minimum grain size (g.s.) and secondary phases of the ZrB_2-based materials. Porosity is estimated by image analysis. SPS: spark plasma sintering, HP: hot pressing, PS: pressureless sintering.

Nonetheless, Fig. 1a shows that about 4 vol% residual rounded closed porosity, with mean size around 4.9 µm, remained trapped within ZrB_2 grains. In addition, the latter ones display quite larger dimensions, around 20 µm, with the maximum size being up to 34 µm. This outcome is likely a consequence of the relatively coarser SHS powders used for SPS experiments with respect to commercial raw ZrB_2 material alternatively utilized in the present study, i.e. 6.7 µm and 2.8 µm mean sizes, respectively.

Finer starting powder and the addition of $MoSi_2$ enabled to reduce surface porosity in the sintered samples, when using either a pressureless oven or a hot pressing furnace, Table I.

In Fig. 1b,c and Fig.2 ZrB_2 exhibits rounded grey grains, while $MoSi_2$ is characterized by brighter contrast and an irregular shape with low dihedral angles. Beside $MoSi_2$ we observed silica pockets

recognizable as dark contrasting phases, often embedding small SiC grains, ZrO_2 and MoB. Formation of these phases during sintering at high temperature is due to $MoSi_2$ reaction with oxygen coming from B_2O_3 present on boride particles surface and subsequent formation of SiO_2 and MoB [20]. Silica is often partially reduced to SiC, due to abundancy of C in graphite-based furnaces. Secondary phases are listed in Table I and, as a consequence of these reactions, the final effective $MoSi_2$ content in the materials containing $MoSi_2$ is slightly different from the nominal one. The matrix mean grain size of the hot pressed ZBMX materials, whose microstructure overview is displayed in Fig. 2, slightly decreased with increasing $MoSi_2$ content, whilst the pores dimension did not notably vary, being around 0.10-0.13 μm, Table I. The grain size is influenced both by decreased sintering temperature, 1900°C for ZBM5 and 1750°C for ZBM50, and by the distribution of $MoSi_2$, which, at high volume fraction, hindered ZrB_2 grains coalescence by creating a continuous interpenetrating network within the boride skeleton, thus obstructing mass transfer. Porosity and mean grain size reduction through $MoSi_2$ addition leads on one side to increased mechanical properties [20], but on the other side spectral selectivity worsens almost linearly with increasing $MoSi_2$, as discussed later.

Fig. 1: SEM images of the surface of various ZrB_2-based ceramics showing different microstructural features. a) ZBM0-s by SHS/SPS, b) ZBM20-ps by pressureless sintering; c) ZBM10 by HP and d) porous ZBM10P by pressureless sintering in presence of pore-generating agent. Pores are marked with dotted circles.

The material produced with the addition of a pore-forming agent ZBM10P, had a surface porosity around 13-15 vol% and displayed a very irregular surface with pore sizes around 3-7 μm, Fig. 1d. The same secondary phases were recognized as for the dense composites produced by hot pressing.

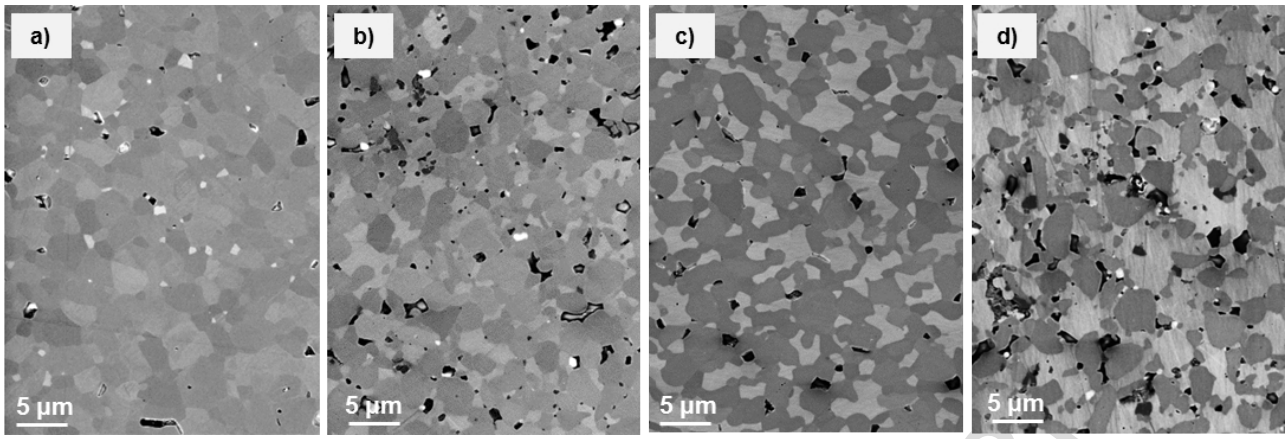

Fig. 2: SEM images of the polished surfaces of hot pressed ZrB_2-based composites with increasing $MoSi_2$ amount: a) 5 vol%, b) 20 vol%, c) 30 vol% and d) 50 vol%.

Etched surface - To increase the capability to trap solar radiation, chemical etching was performed in a HNO_3/HF solution on the ZBM10 sample. X-ray diffraction analysis on the chemically etched surface (not shown), ZBMetc, revealed that only hexagonal ZrB_2 and tetragonal $MoSi_2$ were indexed, with no additional oxides or reaction products formed upon the chemical corrosion. The microstructure of the etched surface is reported in Fig. 3. It can be seen that the chemical treatment effectively etched the surface creating faceted acicular ZrB_2 grains, while leaving $MoSi_2$ unchanged with its pristine smooth contours (compare Fig. 1c and Fig. 3a). Noteworthy, the phase composition did not undergo modification and no contamination by oxygen, fluorine or nitrogen was detected on the etched surface, as demonstrated by the EDS spectra reported in Fig. 3c.

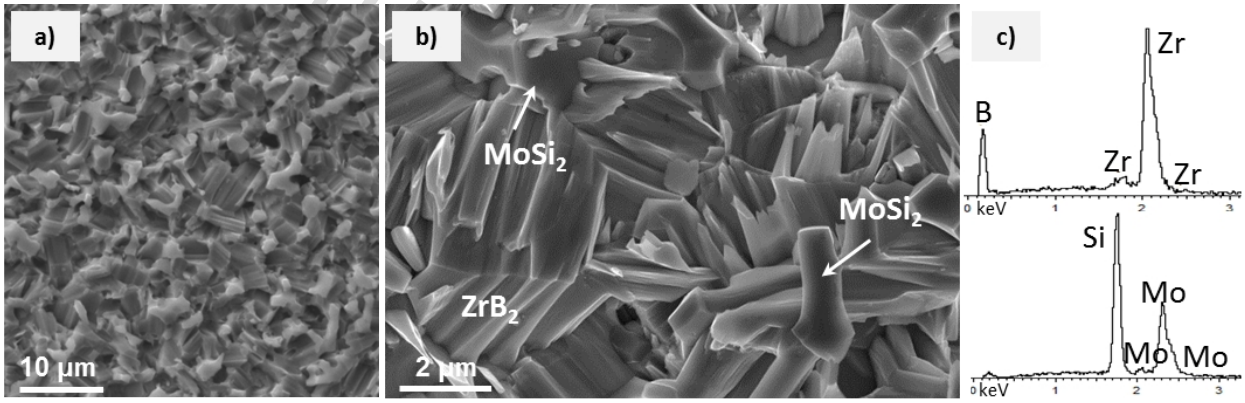

Fig. 3: a)-b) SEM images of the chemically etched surface of ZBM10 with corresponding EDS spectra in c).

Oxidized surfaces - The oxidized ZBM10 samples showed a remarkably changed surface with a glassy appearance. The X-ray diffraction patterns after oxidation at 800 and 1200°C are reported in Fig. 4a. At the lowest temperature, the crystalline phases detected are monoclinic ZrO_2, the pristine ZrB_2 and $MoSi_2$, whilst tetragonal MoB is found instead of ZrB_2 when the oxidation process was conducted at the highest thermal level. To note that a preferential orientation of ZrO_2 phase along the [002] planes at $2\theta=34°$ took place upon exposure at 1200°C, instead of preserving the nominal peak intensity 100% corresponding to the [-111] planes at $2\theta=28°$. Future optical measurements will show if this change of grains orientation has an impact on the solar absorbance.

SEM images of the oxidized surfaces are shown in Fig. 4b-g. At 800°C, Fig. 4b-d, the sample is covered by a continuous boro-silicate glassy layer, which incorporates B_2O_3 crystals and bright ZrO_2 agglomerates, 10-20 μm sized. Cracks in the glass are presumably formed upon cooling. At 1200°C, Fig. 4e-g, the outer scale is mainly based on silica, without boron traces, and contains about 5 μm-sized ZrO_2 agglomerates, where the MoO_3 phase, with white contrast, is disposed intergranularly, Fig. 4g.

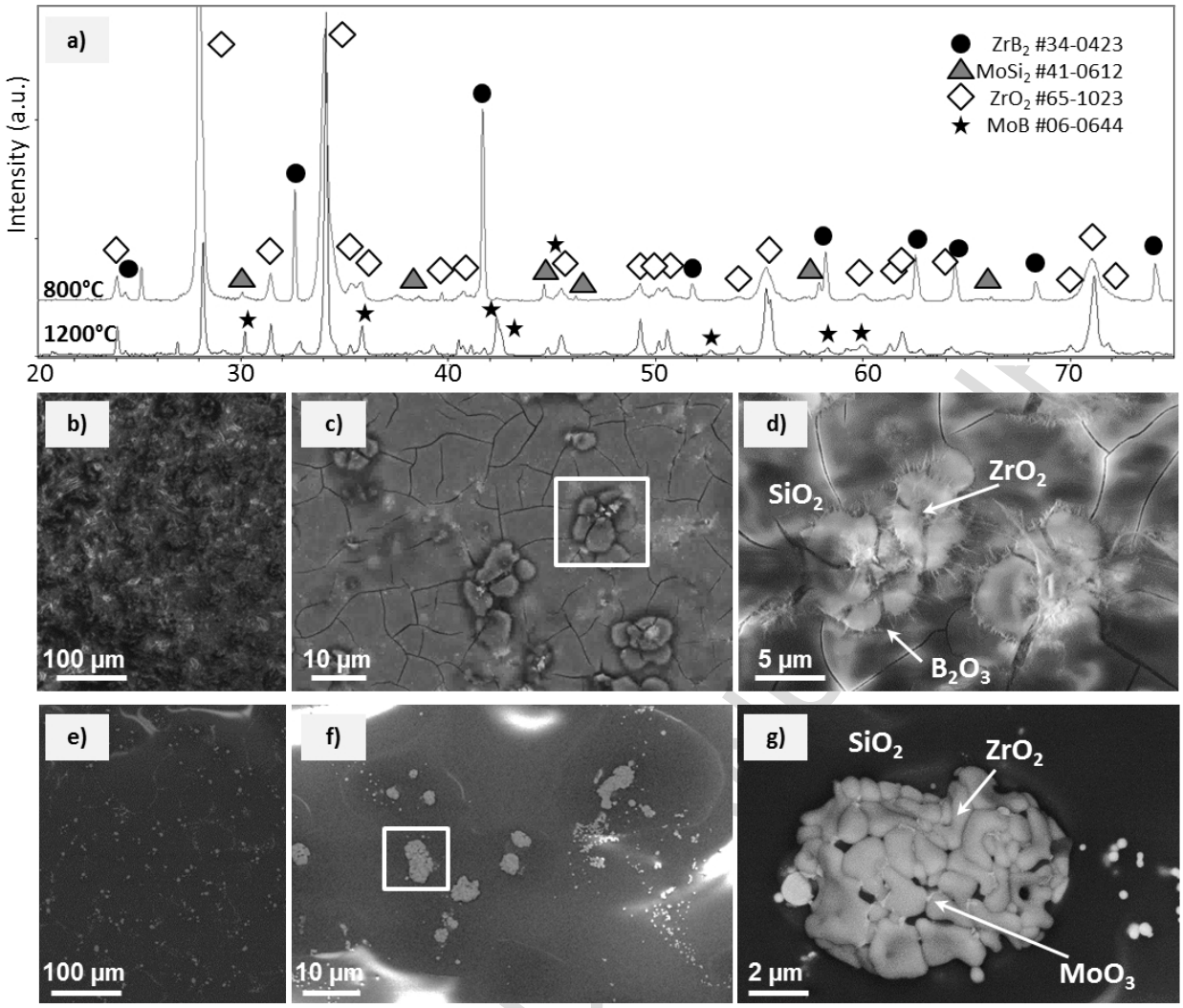

Fig. 4: a) X-ray diffraction patterns of ZBM10 upon exposure to oxidizing environment at 800°C and 1200°C for 10 hours and corresponding SEM images of the external surface oxidized at b)-d) at 800°C and e)-g) 1200°C. d) and g) are magnified images of the boxed areas in c) and f), respectively.

3.2 Surface texture characterization

The surface texture has significant effects on surface absorbance and reflectance, therefore, in order to investigate the intrinsic optical properties of the synthetized materials and evaluate the contributions arising from surface texturing treatment, each sample was characterized from a topological point of view before performing optical measurements.

The surface texture was characterized by evaluating the areal height parameters (Sa, Sq, Ssk, Sku, Sp, Sv and Sz) on the L-filter surface. These parameters provide useful information about the

optical characteristics of a surface, indeed, Sa is related to the surface roughness, Sq to the way in which light is scattered from a surface, while Ssk and Sku are correlated to the type of defects and to their distribution on the samples surface. In particular, negative values of Ssk indicate the predominance of pores or valleys, while large and positive values (> 3) of Sku indicate the presence of a certain amount of high peaks or deep valleys/pores. [30].

In Table 2 the average values of the areal height parameters measured on the studied samples, along with the corresponding standard deviation, are reported.

With the exception of ZBM800, ZBM1200, all the tested specimens showed negative values of Ssk and values of Sku higher than 3. This result indicates that the surface of these samples is characterized by the presence of comparatively few peaks and by the prevalence of quite pronounced pores or valley. These findings are in agreements with the higher values of Sv with respect of Sp detected on these samples. This surface morphology can induce significant improvements to the surface absorbance since it can trap the incident photons and promote their absorption through multiple reflections along the walls of the pore or valley. The relatively high dispersion measured on Ssk and Sku is related to the fact these parameters are very sensitive to surface defects since, in their mathematical expression, high order powers of surface heights are used.

Sa and Sq values for the ZrB_2-based composites follow similar trend on all the tested materials. In particular, hot pressed and pressureless sintered materials showed comparable values of both these parameters. Small variations observed are probably due to differences in surface finishing obtained on samples with different composition.

Higher values of Sa and Sq measured on SPS are probably due to the higher surface porosity (4%) observed on this sample. When the bulk porosity increases over 10%, in the case of ZBM10P, and the porosity changed from close to open, the surface becomes very rough and Sa and Sq increase accordingly about 2 orders of magnitude.

The chemical etching induced significant surface modifications on ZBM10, as highlighted in Figure 3. On ZBMetc, both Sa and Sq increased more than one order of magnitude in comparison

285 with the polished ZBM10 sample while the Ssk and Sku parameters showed a slight decrease in
286 absolute values indicating a bumpy surface morphology.
287

	Polished							Porous	Etched	Oxidised	
	ZBM0-s	ZBM5	ZBM10	ZBM20	ZBM30	ZBM50	ZBM20-ps	ZBM10-P	ZBM Etc	ZBM 800	ZBM 1200
Sq (µm)	0.44±0.10	$(68\pm4)\cdot10^{-3}$	$(34\pm3)\cdot10^{-3}$	$(12\pm3)\cdot10^{-3}$	$(16\pm1)\cdot10^{-3}$	$(22\pm1)\cdot10^{-3}$	$(37\pm10)\cdot10^{-3}$	1.72±0.02	0.69±0.01	0.5±0.3	5.6±4.3
Ssk	-7.1±1.1	-2.4± 0.7	-1.2±0.5	-4.5±2.1	-3.8±0.4	-6.1±1.6	-6.7±1.2	-4.3±0.1	-0.7±0.1	0.9±2.4	1.1±0.9
Sku	83±15	12±4	8±3	81±60	36±5	80±40	97±28	16.3±0.6	3.3±0.6	29±12	5.9±1.6
Sp (µm)	0.8±0.1	5.9±3.5	0.27±0.01	0.21±0.15	0.21±0.01	0.21±0.01	0.28±0.01	8.4±2.9	3.0±1.7	9.8±2.6	46±33
Sv (µm)	9.6±2.5	4.1±2.7	0.51±0.18	0.63±0.46	0.44±0.04	0.70±0.20	1.47±0.74	25.3±0.2	5.5±1.5	9.3±10	11.6±1.1
Sz (µm)	10.4±2.7	10.1±3.1	0.8±0.2	0.8±0.6	0.66±0.04	0.9±0.2	1.8±0.7	33.6±3.3	8.5±3.1	19.1±8.8	57±34
Sa (µm)	0.21±0.28	$(33\pm4)\cdot10^{-3}$	$(25\pm2)\cdot10^{-3}$	$(8\pm2)\cdot10^{-3}$	$(100\pm1)\cdot10^{-4}$	$(12\pm1)\cdot10^{-3}$	$(17\pm4)\cdot10^{-3}$	1.16±0.01	0.57±0.01	0.36±0.18	4.2±3.2

288 Table II: Measured average values and standard deviation of 3D surface texture parameters of the polished and textured
289 (porous/etched/oxidized) ZrB_2-based composites.
290

291 In the case of oxidized samples, a completely different surface morphology was observed. The
292 presence of large and irregular oxidation products, fashioned a surface texture characterized by the
293 prevalence of high irregular peaks in agreement with high values of Sq and Sa and with the positive
294 values of Ssk and Sku parameters. For a more immediate and straightforward comparison, topography
295 maps of the pristine and treated surface are shown in Fig. 5.

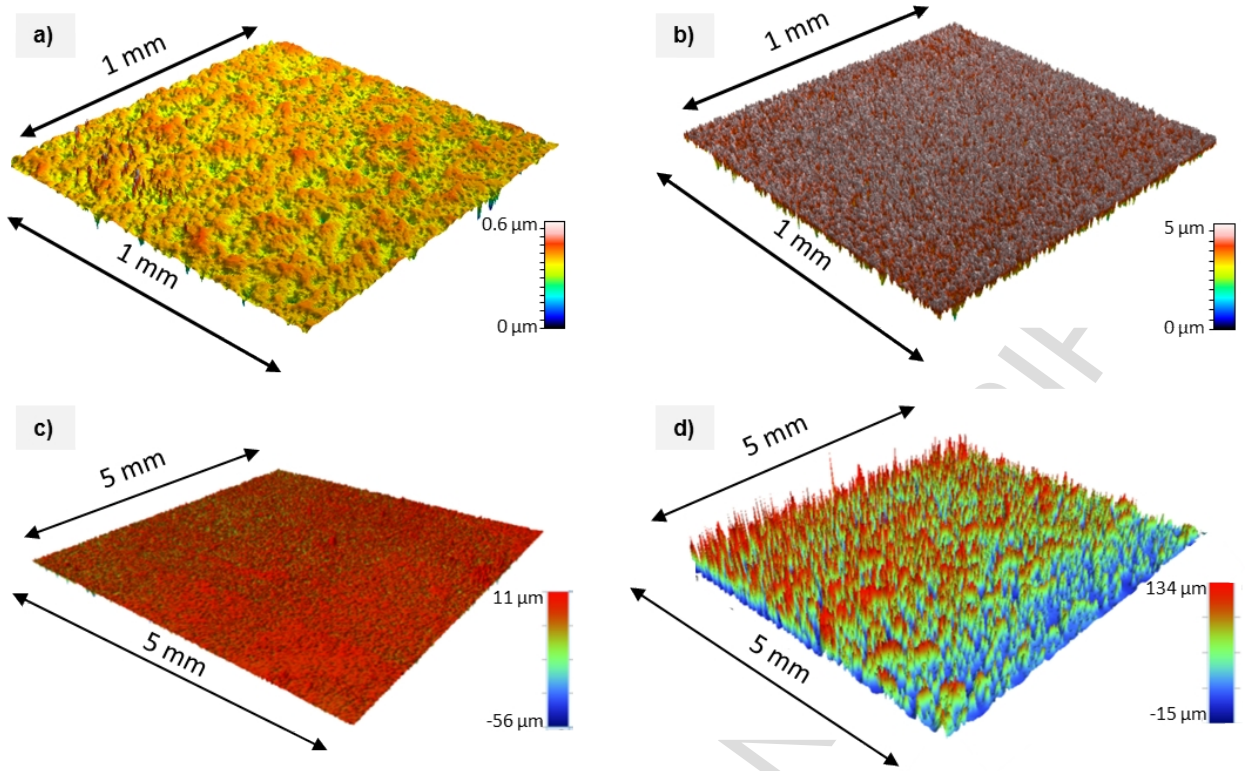

Fig. 5: Topographic maps of the ZBM10 sample upon different surface finishing a) as-polished, b) chemically etched (ZBMetc), c) oxidized at 800°C (ZBM800) and d) oxidised at 1200°C (ZBM1200) for 10 hours.

3.4 Optical characterization

In agreement with previous investigations [13,14,16,17,28], ZrB_2 composites have a step-like optical behaviour. In this regard, Fig. 6a displays the hemispherical reflectance spectra shown by the additive free SPSed sample and the hot pressed ZBMX composites with increasing $MoSi_2$ content, together with that of SiC, reported for the sake of clarity as reference material. We can distinguish the typical step-like behaviour of ZBMX samples as well and similar maximum reflectance among samples, which is around 85-90%. ZBMX spectra have very similar shape, with the highest values for ZBM0-s and ZBM5 especially at short wavelengths. The typical $MoSi_2$ reflectance minimum at 2.7 µm already appears in the spectrum of ZBM5 and progressively increases proportionally with the additive content. The bump at around 9 µm, attributable to SiO_2 signal, can be clearly identified only in ZBM30 and ZBM50, in agreement with their much higher SiO_2 content than the other hot pressed

311 materials. Completely different spectral characteristics of borides over SiC are well discernible in
312 Fig. 6a.

313 Fig. 6b evidences that no significant differences in optical spectra can be connected to the
314 processing technique for ZBM20 samples, either hot pressing and pressureless sintering. Fig. 6c
315 compares dense and porous ZBM10 obtained by hot pressing (blue and green curves, respectively),
316 and the dense sample before and after chemical etching (blue and red curves, respectively). Porosity
317 shows a clear effect in reducing the spectral reflectance with respect to the fully dense sample. On
318 the other hand, the radical change of surface morphology after chemical etching, inducing an increase
319 of roughness, also determined a significant decrease of the reflectance over the whole wavelength
320 examined. This holds particularly true in the intervals of major interest, i.e. for wavelengths lower
321 than 1 μm and between 1 and 3 μm. In detail, it passes from around 50% in the visible-near IR and
322 50-80 % in the range 1-3 μm for the polished pristine surface to around 25 % and 25-40 % for the
323 textured surface in the two investigated ranges (Fig. 6c). As X-ray analyses revealed the presence of
324 solely ZrB_2 and $MoSi_2$ in the etched sample, the local minimum in the range 6-8 μm in the reflectance
325 curve of the etched ZBM10 is likely connected to the textured morphology of the surface rather than
326 to the presence of oxides. In fact, surface texturing has been proved in the literature to strongly affect
327 optical reflectance properties of solids [31–33].

328 Finally, the optical spectra of the oxidized samples in Fig. 6d result completely changed
329 compared with the pristine material. Indeed, whilst the XRD are still able to detect ZrB_2 under the
330 silica coverage after oxidation at 800°C, the optical spectrum only shows the surficial nature of the
331 material, e.g. the newly formed silica scale. The spectrum observed in Fig. 6d well compares with
332 that of amorphous SiO_2, as this is the main phase composing the outermost surface scale as discussed
333 above (Fig. 4b-c). It should be noticed that the same situation is produced upon SiC exposure to high
334 temperatures in air.

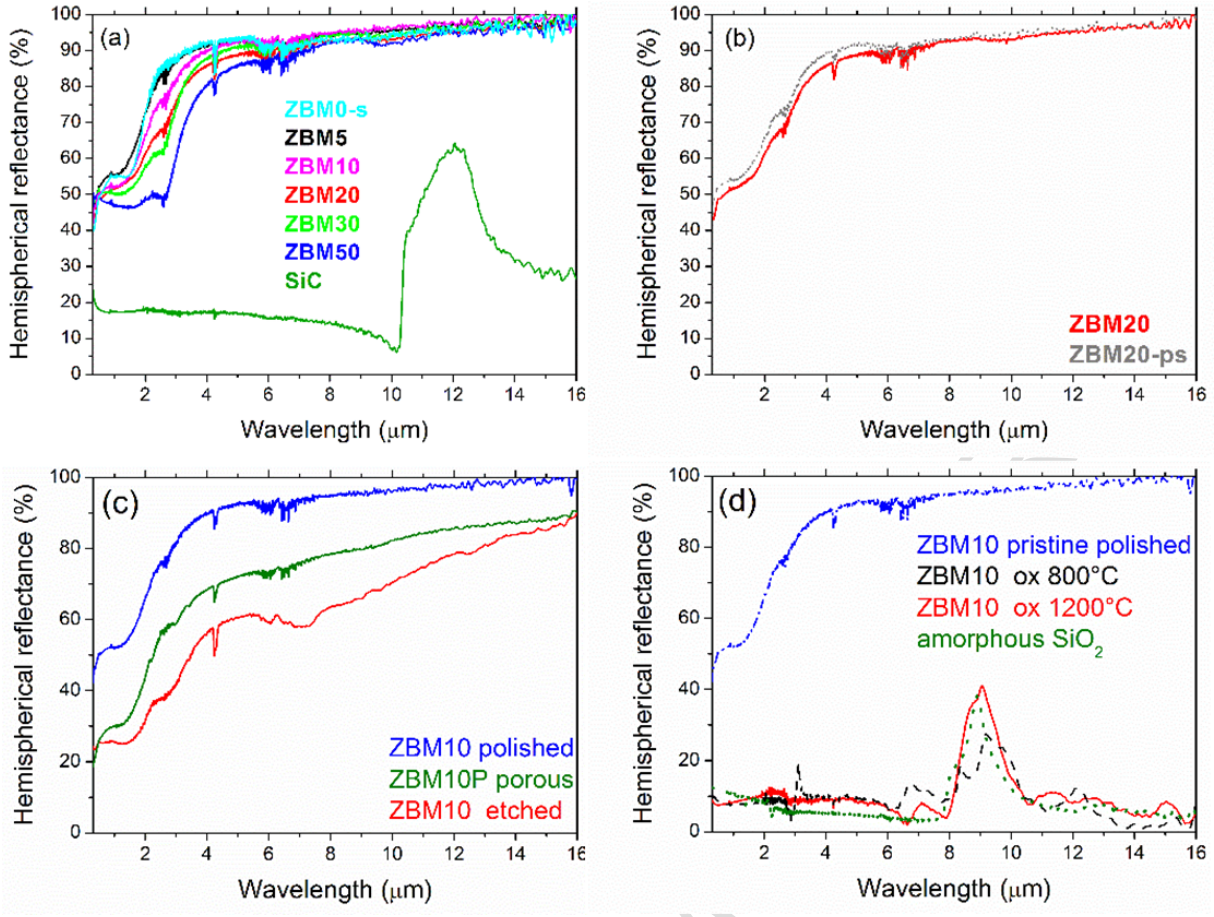

Fig. 6: a) Comparison of hemispherical reflectance spectra of hot pressed ZrB_2 materials as a function of the additive amount. The spectrum of SiC is also shown for reference. b) Comparison between the two samples with 20% $MoSi_2$ as a function of the processing technique. c) Comparison between the spectra of dense, porous and etched ZBM10. d) Comparison amongst polished and oxidized ZBM10 samples at 800 or 1200°C, together with that of a reference amorphous SiO_2.

Experimental emittance spectra at 1100 K of dense and porous samples, ZBM10 and ZBM10P, are shown in Fig. 7 and compared to the emittance of a SiC sample. The drop in SiC emittance at around 12 μm wavelength is due to intrinsic spectral characteristics of the material (see also Fig. 6a) and it represents the Reststrahlen band [34]. Boride spectra are very similar to each other and significantly lower than that of SiC. The two ZBM10 spectra cross at around 10 μm wavelength, with the dense sample showing a slightly higher spectral curve than the porous one at shorter wavelengths. This result at a first glance could seem counter-intuitive. In fact, it could seem reasonable to expect a clearly higher thermal emittance of the porous sample than the dense one, as

it happens in samples with similar surface roughness or when a denser sample is also smoother [35,36]. However it should not be forgotten that thermal emittance is a surface property, thus it is the result of the overall balance of all the parameters of the surface. In our case, the samples have a different surface finishing. In particular, the dense ZBM10 has a higher roughness than the porous ZBM10P pellet. The balance between roughness and porosity effects fairly justifies the observed similarity of emittance. Finally, it should be noted, that the small spectral differences outlined above do not produce significant differences on the value of the spectrally-integrated emittance ($\varepsilon_{exp} \approx 0.3$ for both borides). On the other hand, SiC, which has a roughness similar to that of ZBM10, exhibits a markedly higher emittance than borides in the large majority of the spectrum. Accordingly, the corresponding integrated value is more than double ($\varepsilon_{exp} \approx 0.8$).

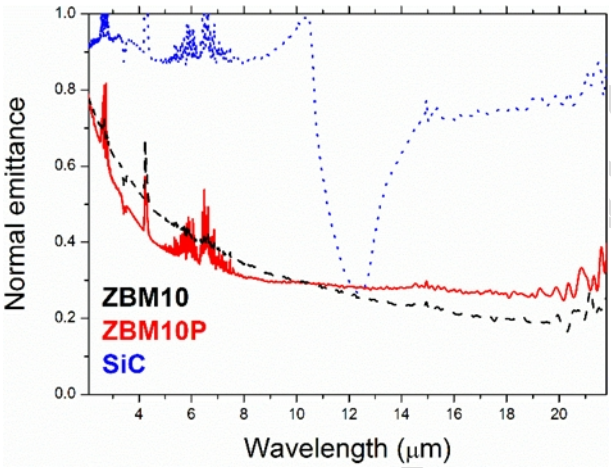

Fig.7: Comparison of the spectral normal emittance of ZBM10 samples and SiC at 1100 K. Due to thermal contact losses at the ceramic pellet/heater interface, 1100K is the maximum temperature actually obtained for these samples. Spectral features at around 2.5, 3, 4 and 6 μm wavelength, which are shown by all samples, are instrumental artifacts due to unbalanced absorption by air gases.

4. Discussion

4.1 Bulk and surface features affecting the optical behavior

One of the main objectives of this work is understanding what are the most important microstructural characteristics affecting the optical behaviour. The fundamental parameters we have considered are α and α/ε that, ideally, should be as closer to one and as higher as possible,

respectively. For the sake of comparison, we have indicated the same parameters for a hot pressed SiC reference material. SiC typical values of α and α/ε are 0.8 and 1, respectively.

Effect of secondary phases: The experiments conducted indicate that the intrinsic spectral behaviour of these multiphase materials is affected by the presence of secondary phases such as $MoSi_2$, e.g. by the chemical composition of the final product. To note that the introduction of a specific sintering agent is often mandatory if we want to exploit the full potential of ZrB_2 as structural ceramic and improve its oxidation behaviour [20]. For the optical behaviour, we showed that even a content as low as 5 vol% of $MoSi_2$ in a ZrB_2 matrix (ZBM5) produces some change in the optical spectrum, compared to the $MoSi_2$-free material (ZBM0-s). Similarly, the presence of silica, in amount >5 vol% is also detected in the spectra. In the specific case of $MoSi_2$, the change of hemispherical reflectance is observed mostly in the 0.3-3 micron wavelength range, Fig. 6a, but the overall hemispherical solar absorbance (Eq. 1), plotted in Fig. 8a as a function of $MoSi_2$ content, just shows a slight increase from 0.44 to 0.52 for $MoSi_2$ content increasing from 0 to 50%. This absorbance increase is beneficial for solar energy application, but α remains still lower than SiC. On the other hand, for α/ε the variability range lies between 1.7 for ZBM50 and 3.1 for ZBM0-s, Fig. 8b. It clearly looks that spectral selectivity worsens almost linearly with increasing $MoSi_2$ and related secondary phases, like SiO_2. As term of comparison, it should be recalled that SiC calculated α/ε ratio is about 1, which is always lower than all ZBMX products.

It is immediate here to notice the dichotomy connected with the decrease of reflectance and its effects on α and α/ε parameters. In fact, due to spectral properties of UHTCs, it is quite a common result that a reflectance decrease entails the growth of both α and ε parameters, with a subsequent decrease in α/ε ratio. However, some authors underlined the importance of a high absorbance value for spectrally selective absorbers [5]. Thus, as a phenomenological rule of thumb, providing that the spectral selectivity is maintained (i.e. α/ε >1), a higher absorbance should be preferred, even at the cost of some decrease of spectral selectivity. The spectral selectivity, however, should not be completely lost, because, as the cited paper proves [5], selective absorbers always show better performances than

non-selective materials, even if they are characterized by a high absorbance (e.g. SiC, α/ε=1).

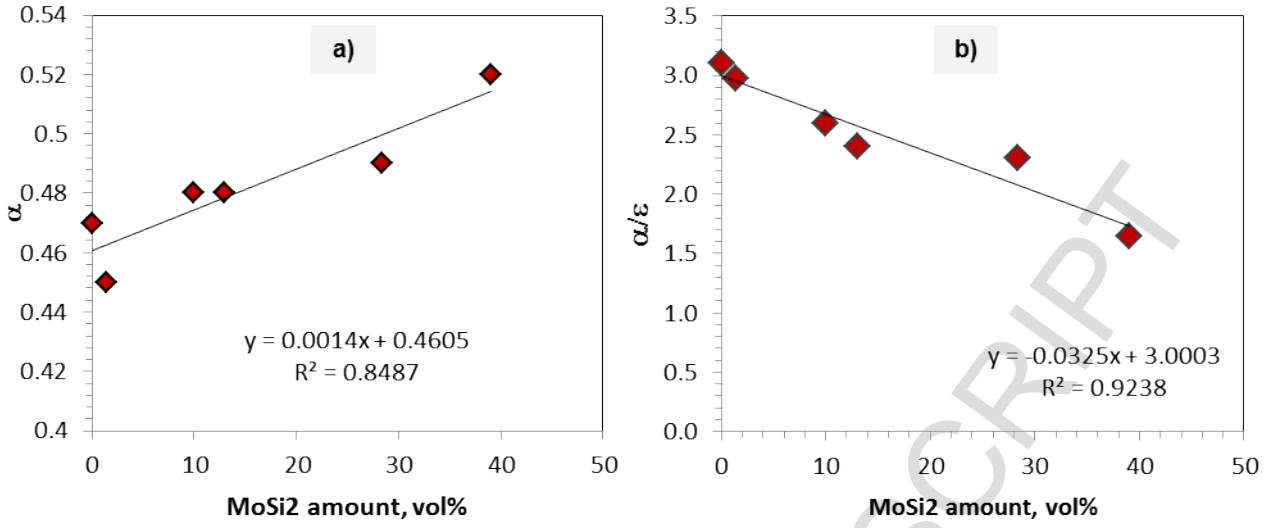

Fig. 8: a) Solar absorbance, α, and b) Spectral selectivity, α/ε, for the series ZBMX, dense samples.

Effect of surface porosity: Further, surface morphology is the other fundamental parameter affecting the optical behavior. We have shown that playing with surface porosity we can achieve a drastic change of the optical spectrum. Increase of porosity over 10%, does not substantially change the spectrum shape as we still observe the spectral selectivity of the boride phase, but produces a large increase of the absorbance. If we use the roughness as a quantitative parameter, we can say that variations of at least one order of magnitude in surface roughness result in significant change of α and α/ε. Therefore, increased roughness leading to improved capability to trap solar radiation could be tailored mainly by augmenting the surface porosity. This can be accomplished through addition of pore forming agents, with the possibility to decide *a priori* the pore dimensions, or modifying the sintering schedule to avoid complete densification.

Effect of surface etching: If α and α/ε values are concerned, Fig. 9, we can see that surface etching increases the absorbance, which is nearly doubled, and decreases the spectral selectivity correspondingly, similarly to that obtained in the case of femtosecond-treated materials [31]. It is worth to mention that the absorbance value obtained for the etched sample is very similar to that of silicon carbide, thus overcoming one of the major criticisms for UHTC materials over SiC itself. On

the other hand, the spectral selectivity of etched ZrB_2 remains better. Therefore, these results confirm that surface texturing is a successful approach for developing promising solar absorbers, according to the criteria described in [5].

Effect of surface oxidation: As expected, optical properties of oxidized samples deteriorate due to the complete change of surface composition and morphology with respect to the pristine boride, in agreement with the findings of other authors [37]. However, they still remain comparable to SiC, both in terms of values of the optical parameters and also because, as mentioned before, SiC itself shows a similar oxidation behavior, with the production of an amorphous silica layer on the exposed surface.

As a final comment about emittance measurements, it is a known effect that the experimental emittance at high temperature is generally higher than the value estimated from room-temperature reflectance spectra using Eq. (2) [28]. However, as discussed in the cited work, the parameters α and α/ε obtained from the room-temperature optical characterization remain valid if the obtained results are used for comparison among samples, as the hierarchy and relative differences among specimens are kept the same, both in low and high temperature measurements.

4.2 Advantages in the use of UHTC as solar absorbers

The need to identify suitable strategies to halve the cost of energy production from CSP technologies has fostered research effort aiming at developing materials for alternative, sustainable, safe and cost-effective energy supply.

In this context, innovative materials have been investigated within the SUPERSOLAR project. In particular, a thorough knowledge of the relationship between processing, microstructure, thermo-mechanical and optical properties has been assessed for the first time for UHTC materials. The base properties outlined in this and previous studies [13,14,16,17,28] can be the starting point for future development of ground-breaking materials with specific properties tunable according to the needs imposed by the application.

The investigations performed so far underlined solar energy relevance as future main energy supply through the use of UHTCs as innovative materials for solar absorbers. In particular, the following two aspects have been tackled:

- Development of new more efficient systems. From the point of view of materials design and production, particular attention has been devoted to the selection of ceramics of the UHTC class possessing superior durability and high temperature stability, able to operate at higher temperatures, as compared to the actual materials based on SiC; appropriate surface treatments have been also performed to enhance the materials absorbance.
- Reduction of materials production costs through the employment of cost-effective processing techniques. In this respect, SHS/SPS and pressureless sintering routes have been also explored beside the conventional hot pressing technique.

In particular, the SHS/SPS approach contemplates several advantages: a possible cost-production saving could be achieved by the use of raw powders obtained through in-house synthesis; in addition, SPS has the benefit to reduce the sintering times from the order of hours to minutes. On the other hand, sintering performed without the application of pressures enables the obtainment of near-net shape components, thus saving machining costs.

4.3 Strengths and criticalities of UHTCs as solar absorbers

A clearer picture of the complex relationships amongst process-microstructure-optical properties of UHTCs can be defined taking advantage of our experience gained in recent years on this subject [13,14,16,17,28]. In particular, the research activity revealed interesting findings, but also pointed out some critical issues in the use of UHTCs as solar absorbers.

The main strength point is that the optical behaviour of all materials analysed favourably competes with that of SiC, which is the most widespread material used for current applications. Not to forget that also the mechanical properties and refractoriness of UHTCs are generally higher than those of SiC materials, as well. Then, the high thermal conductivity of UHTCs, between 60 and 100

468 $Wm^{-1} K^{-1}$ and constant up to 1500°C [38,39] is even higher than SiC, 4-20$Wm^{-1} K^{-1}$ [40] allowing
469 for an easy heat transfer of the collected thermal energy to a thermo-convective fluid.

470 Further, the surface treatments experimented in the study, chemical etching and tailored
471 porosity, proved to effectively decrease the reflectance in the visible-near infrared spectral range, i.e.
472 increased the ability of the material to absorb the incident radiation, which can be translated in higher
473 efficiency of the system.

474 One not-negligible problem is related to the cost of the starting powders. UHTC powders are
475 consistently more expensive than SiC ones. However, in this study we demonstrated the feasibility
476 of UHTCs starting from in-house reaction synthesized powders, that enabled to save costs as
477 compared to commercial ones. More important, the maximum temperature required for their
478 densification is generally lower than that required for commercial UHTC powders, as the SHS
479 powders are easily sinterable owing to the high defects concentration. One further step towards the
480 decrease of the sintering temperatures is constituted by the fact that partially porous materials possess
481 lower reflectance, thanks to an increased absorption capability of the material, as the solar radiation
482 is more easily trapped into the channels created by porosity.

483 Moving to the critical aspects of the use of UHTCs as solar absorbers for novel high-temperature-
484 high-efficiency solar plants, the last investigations on the behaviour of oxidized ceramics pointed out
485 that the transition from boride to oxide, zirconia or silica, has notable impact on the optical response,
486 see Fig. 6b. This leads to conclude that the use of these materials at high temperature is subordinated
487 to a protective/reducing environment. However, it is worth to recall that, on a side, SiC also shows
488 oxidation problems and, on the other side, oxidized borides show α/ε values comparable to SiC,
489 whereas α parameters are even better than this reference material, see Fig. 9.

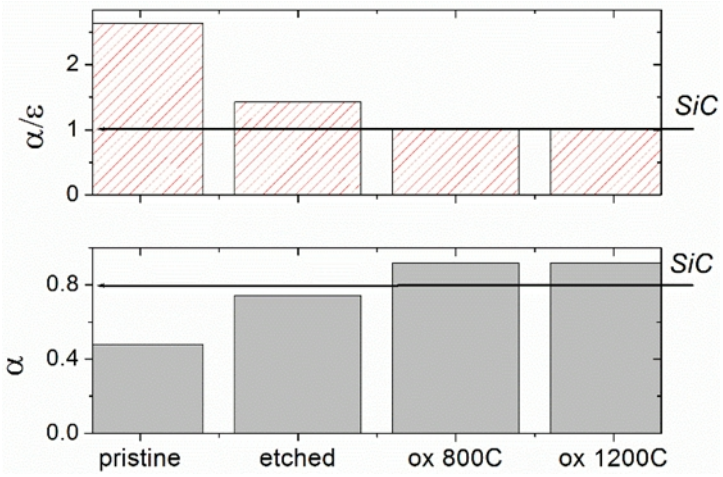

Fig. 9: Spectral selectivity, α/ε, and solar absorbance, α, for the pristine and treated samples. Horizontal lines in each plot identify the values obtained for SiC.

5. Conclusions

The investigations on a broad range of UHTCs allowed to assess that these materials used in this novel application as solar absorbers well compare and even overpass the performances of more conventional SiC-based materials both at room and high temperatures. Zirconium diboride has been taken as case study and thoroughly characterized as a function of starting composition, porosity and surface finishing. Surface texturing by chemical etching has been investigated, showing increased solar absorbance. Oxidation has shown significantly changed material properties, making borides behave more similar to SiC. Finally, thermal optical spectra at 1100 K temperature have been acquired and compared to SiC, confirming the trend revealed by room-temperature optical parameters.

Acknowledgements

This activity has been carried out in the framework of the FIRB2012-SUPERSOLAR project funded by the Italian Ministry of University and Research (Programma “Futuro in Ricerca”, prot. RBFR12TIT1). The Italian bank foundation “Fondazione Ente Cassa di Risparmio di Firenze” is gratefully acknowledged for supporting a part of this activity within the framework of the SOLE-NANO project (pratica n. 2015.0861). Thanks are due Mr. M. Pucci, Mr. M. D’Uva (CNR-INO), Mr.

Cesare Melandri (CNR-ISTEC) for technical support and to Mrs. R. Parenti and Mrs. P. Pipino (CNR-INO) for administrative management.

References

[1] Romero M, Steinfeld A. Concentrating solar thermal power and thermochemical fuels. Energy Environ Sci 2012;5:9234. doi:10.1039/c2ee21275g.

[2] Bogaerts WF, Lampert CM. Materials for photothermal solar energy conversion. J Mater Sci 1983;18:2847–75. doi:10.1007/BF00700767.

[3] Lampert CM. Advanced optical materials for energy efficiency and solar conversion. Sol Wind Technol 1987;4:347–79. doi:10.1016/0741-983X(87)90067-1.

[4] Kennedy C. Review of mid-to high-temperature solar selective absorber materials. NREL Tech Rep 2002:1–58. doi:10.2172/15000706.

[5] Burlafinger K, Vetter A, Brabec CJ. Maximizing concentrated solar power (CSP) plant overall efficiencies by using spectral selective absorbers at optimal operation temperatures. Sol Energy 2015;120:428–38. doi:10.1016/j.solener.2015.07.023.

[6] Patidar D, Tiwari S, Sharma PK, Chandra L, Shekhar R. Open Volumetric Air Receiver Based Solar Convective Aluminum Heat Treatment Furnace System. Energy Procedia, vol. 69, 2015, p. 506–17. doi:10.1016/j.egypro.2015.03.059.

[7] Srivastva U, Malhotra RK, Kaushik SC. Recent Developments in Heat Transfer Fluids Used for Solar Thermal Energy Applications. J Fundam Renew Energy Appl 2015;5. doi:10.4172/20904541.1000189.

[8] Stadler H, Tiddens A, Schwarzbözl P, Göhring F, Baumann T, Trautner J. Improved performance of open volumetric receivers by employing an external air return system. Sol Energy 2017;155:1157–64. doi:10.1016/j.solener.2017.07.050.

[9] Zhu G, Libby C. Review and future perspective of central receiver design and performance. AIP Conf. Proc., vol. 1850, 2017. doi:10.1063/1.4984395.

[10] Wuchina EJ, Opila E, Opeka M, Fahrenholtz WG, Talmy I. UHTCs: Ultra-high temperature ceramic materials for extreme environment applications. Electrochem Soc Interfaces 2007;16:30–6.

[11] Silvestroni L, Kleebe H-J, Fahrenholtz WG, Watts J. Super-strong materials for temperatures exceeding 2000 °C. Sci Rep 2017;7:40730. doi:doi:10.1038/srep40730.

[12] Fahrenholtz WG, Wuchina EJ, Lee WE, Y. Z, editors. Ultra-High Temperature Ceramics: Materials for Extreme Environment Applications. John Wiley & Sons; 2014.

[13] Sani E, Mercatelli L, Meucci M, Balbo A, Silvestroni L, Sciti D. Compositional dependence of optical properties of zirconium, hafnium and tantalum carbides for solar absorber applications. Sol Energy 2016;131:199–207. doi:10.1016/j.solener.2016.02.045.

[14] Sani E, Mercatelli L, Meucci M, Silvestroni L, Balbo A, Sciti D. Process and composition dependence of optical properties of zirconium, hafnium and tantalum borides for solar receiver applications. Sol Energy Mater Sol Cells 2016;155:368–77. doi:10.1016/j.solmat.2016.06.028.

[15] Musa C, Licheri R, Orrù R, Cao G, Sciti D, Silvestroni L, et al. Processing, mechanical and optical properties of additive-free ZrC ceramics prepared by Spark Plasma Sintering. Materials (Basel) 2016;9. doi:10.3390/ma9060489.

[16] Sani E, Mercatelli L, Meucci M, Balbo A, Musa C, Licheri R, et al. Optical properties of dense zirconium and tantalum diborides for solar thermal absorbers. Renew Energy 2016;91:340–6. doi:10.1016/j.renene.2016.01.068.

[17] Sani E, Meucci M, Mercatelli L, Balbo A, Musa C, Licheri R, et al. Titanium diboride ceramics for solar thermal absorbers. Sol Energy Mater Sol Cells 2017;169:313–9. doi:10.1016/j.solmat.2017.05.038.

[18] Sani E, Mercatelli L, Meucci M, Zoli L, Sciti D. Lanthanum hexaboride for solar energy applications. Sci Rep 2017:1–7. doi:10.1038/s41598-017-00749-w.

[19] Rousseau B, Guevelou S, Vicente J, Caliot C, Flamant G. Tuning the Spectral Selectivity of

562 Sic-Based Volumetric Solar Receivers With Ultra-High Temperature Ceramic Coatings.
563 Ceram. Energy Conversion, Storage, Distrib. Syst., vol. 255, 2016, p. 227–38.
564 doi:10.1002/9781119234531.ch21.
565 [20] Sciti D, Silvestroni L, Medri V, Monteverde F. Sintering and Densification Mechanisms of
566 Ultra-High Temperature Ceramics. 2014. doi:10.1002/9781118700853.ch6.
567 [21] Neuman EW, Hilmas GE, Fahrenholtz WG. Processing, microstructure, and mechanical
568 properties of zirconium diboride-boron carbide ceramics. Ceram Int 2017;43:6942–8.
569 doi:10.1016/j.ceramint.2017.02.117.
570 [22] Neuman EW, Hilmas GE, Fahrenholtz WG. Processing, microstructure, and mechanical
571 properties of large-grained zirconium diboride ceramics. Mater Sci Eng A 2016;670:196–
572 204. doi:10.1016/j.msea.2016.06.017.
573 [23] Farahbakhsh I, Ahmadi Z, Shahedi Asl M. Densification, microstructure and mechanical
574 properties of hot pressed ZrB2–SiC ceramic doped with nano-sized carbon black. Ceram Int
575 2017;43:8411–7. doi:10.1016/j.ceramint.2017.03.188.
576 [24] Neuman EW, Hilmas GE, Fahrenholtz WG. Mechanical behavior of zirconium diboride-
577 silicon carbide-boron carbide ceramics up to 2200°C. J Eur Ceram Soc 2015;35:463–76.
578 doi:10.1016/j.jeurceramsoc.2014.09.021.
579 [25] Petrovic JJ. Mechanical behavior of MoSi2 and MoSi2 composites. Mater Sci Eng A
580 1995;192–193:31–7. doi:10.1016/0921-5093(94)03246-7.
581 [26] Sciti D, Silvestroni L, Saccone G, Alfano D. Effect of different sintering aids on thermo-
582 mechanical properties and oxidation of SiC fibers - Reinforced ZrB2 composites. Mater
583 Chem Phys 2013;137:834–42. doi:10.1016/j.matchemphys.2012.09.071.
584 [27] Licheri R, Musa C, Orrù R, Cao G, Sciti D, Silvestroni L. Bulk monolithic zirconium and
585 tantalum diborides by reactive and non-reactive spark plasma sintering. J Alloys Compd
586 2016;663:351–9. doi:10.1016/j.jallcom.2015.12.096.
587 [28] Mercatelli L, Meucci M, Sani E. Facility for assessing spectral normal emittance of solid

588 materials at high temperature. Appl Opt 2015;54:8700. doi:10.1364/AO.54.008700.
589 [29] ASTM G173-03(2012), Standard Tables for Reference Solar Spectral Irradiances: Direct
590 Normal and Hemispherical on 37° Tilted Surface, ASTM International, West Conshohocken,
591 PA, 2012, www.astm.org n.d. doi:DOI: 10.1520/G0173-03R12.
592 [30] Leach R. Characterisation of areal surface texture. vol. 9783642364. 2013. doi:10.1007/978-
593 3-642-36458-7.
594 [31] Sciti D, Silvestroni L, Trucchi DM, Cappelli E, Orlando S, Sani E. Femtosecond laser
595 treatments to tailor the optical properties of hafnium carbide for solar applications. Sol
596 Energy Mater Sol Cells 2015;132. doi:10.1016/j.solmat.2014.09.037.
597 [32] Nayak BK, Iyengar V V., Gupta MC. Efficient light trapping in silicon solar cells by
598 ultrafast-laser-induced self-assembled micro/nano structures. Prog Photovoltaics Res Appl
599 2011;19:631–9. doi:10.1002/pip.1067.
600 [33] King DL, Buck ME. Experimental optimization of an anisotropic etching process for random
601 texturization of silicon solar cells. Conf Rec Twenty-Second IEEE Photovolt Spec Conf -
602 1991 1991:303–8. doi:10.1109/PVSC.1991.169228.
603 [34] Huffmann B and. Absorption and scattering of light by small particles. WILEY-VCH Verlag
604 GmbH & Co. KGaA; 1998. doi:10.1002/9783527618156.
605 [35] Sani E, Mercatelli L, Sans JL, Silvestroni L, Sciti D. Porous and dense hafnium and
606 zirconium ultra-high temperature ceramics for solar receivers. Opt Mater (Amst)
607 2013;36:163–8. doi:10.1016/j.optmat.2013.08.020.
608 [36] Sciti D, Silvestroni L, Sans JL, Mercatelli L, Meucci M, Sani E. Tantalum diboride-based
609 ceramics for bulk solar absorbers. Sol Energy Mater Sol Cells 2014;130:208–16.
610 doi:10.1016/j.solmat.2014.07.012.
611 [37] Charpentier L, Caliot C. The impact of the oxidation on the optical properties of TaC. Sol
612 Energy Mater Sol Cells 2017;171:16–23. doi:10.1016/j.solmat.2017.06.019.
613 [38] Zimmermann JW, Hilmas GE, Fahrenholtz WG, Dinwiddie RB, Porter WD, Wang H.

614 Thermophysical properties of ZrB2 and ZrB2-SiC ceramics. J Am Ceram Soc
615 2008;91:1405–11. doi:10.1111/j.1551-2916.2008.02268.x.
616 [39] Guo S-Q. Densification of ZrB2-based composites and their mechanical and physical
617 properties: A review. J Eur Ceram Soc 2009;29:995–1011.
618 doi:10.1016/j.jeurceramsoc.2008.11.008.
619 [40] Levinshtein ME, Rumyantsev SL, Shur M, Bougrov V, Zubrilov A. Properties of Advanced
620 Semiconductor Materials: GaN, AIN, InN, BN, SiC, SiGe. 2001. doi:citeulike-article-
621 id:6144117.
622
623

Tables

Label	$MoSi_2$ vol%	Sintering technique	T,t,P °C, min, MPa	Bulk relative density %	Surface porosity vol%	Mean pore size µm	Mean g.s. µm	Max g.s. µm	Min g.s. µm	Secondary phases by SEM-EDS vol%
ZBM0-s	0	SPS	1850,20,60	>96	~4	4.90	19±6	33.5	8.5	-
ZBM5	5	HP	1900,10,30	>98	~2	0.13	1.9±0.7	3.6	0.9	1.4 $MoSi_2$, 1.5 SiO_2/SiC
ZBM10	10	HP	1850,10,30	>96	~4	0.13	2.4±0.6	3.9	1.4	8.5 $MoSi_2$, 1.4 SiO_2, 0.7 SiC
ZBM20	20	HP	1800,4,30	>98	~2	0.10	2.4±0.9	5.4	0.6	13 $MoSi_2$, 2.5 SiO_2, 2.0 SiC, 0.7 $ZrO_2$2, 0.6 MoB
ZBM30	30	HP	1850,3,30	>98	~2	0.10	1.7±0.6	3.6	0.6	28.4 $MoSi_2$, 3.4 SiO_2/SiC
ZBM50	50	HP	1750,13,30	>98	~2	0.10	1.9±0.8	4.3	0.7	39 $MoSi_2$, 6.5 SiO_2, 2 MoB, 1 ZrO_2, 1 SiC
ZBM20-ps	20	PS	1950,60,-	>98	~2	1.45	2.6±0.7	1.3	4.1	18 $MoSi_2$, 2 MoB, 0.5 SiO_2
ZBM10P	10	PS	1950,60,-	~87	~13	4.70	2.8±0.7	5.2	1.2	8 $MoSi_2$, 2 MoB

Table I: Composition, sintering technique and parameters, T: maximum temperature, t: dwell at T, P: applied pressure, relative density, porosity features, mean, maximum and minimum grain size (g.s.) and secondary phases of the ZrB_2-based materials. Porosity is estimated by image analysis. SPS: spark plasma sintering, HP: hot pressing, PS: pressureless sintering.

	Polished							Porous	Etched	Oxidised	
	ZBM0-s	ZBM5	ZBM10	ZBM20	ZBM30	ZBM50	ZBM20-ps	ZBM10-P	ZBM Etc	ZBM 800	ZBM 1200
Sq (µm)	0.44±0.10	$(68\pm4)\cdot10^{-3}$	$(34\pm3)\cdot10^{-3}$	$(12\pm3)\cdot10^{-3}$	$(16\pm1)\cdot10^{-3}$	$(22\pm1)\cdot10^{-3}$	$(37\pm10)\cdot10^{-3}$	1.72±0.02	0.69±0.01	0.5±0.3	5.6±4.3
Ssk	-7.1±1.1	-2.4± 0.7	-1.2±0.5	-4.5±2.1	-3.8±0.4	-6.1±1.6	-6.7±1.2	-4.3±0.1	-0.7±0.1	0.9±2.4	1.1±0.9
Sku	83±15	12±4	8±3	81±60	36±5	80±40	97±28	16.3±0.6	3.3±0.6	29±12	5.9±1.6
Sp (µm)	0.8±0.1	5.9±3.5	0.27±0.01	0.21±0.15	0.21±0.01	0.21±0.01	0.28±0.01	8.4±2.9	3.0±1.7	9.8±2.6	46±33
Sv (µm)	9.6±2.5	4.1±2.7	0.51±0.18	0.63±0.46	0.44±0.04	0.70±0.20	1.47±0.74	25.3±0.2	5.5±1.5	9.3±10	11.6±1.1
Sz (µm)	10.4±2.7	10.1±3.1	0.8±0.2	0.8±0.6	0.66±0.04	0.9±0.2	1.8±0.7	33.6±3.3	8.5±3.1	19.1±8.8	57±34
Sa (µm)	0.21±0.28	$(33\pm4)\cdot10^{-3}$	$(25\pm2)\cdot10^{-3}$	$(8\pm2)\cdot10^{-3}$	$(100\pm1)\cdot10^{-4}$	$(12\pm1)\cdot10^{-3}$	$(17\pm4)\cdot10^{-3}$	1.16±0.01	0.57±0.01	0.36±0.18	4.2±3.2

Table II: Measured average values and standard deviation of 3D surface texture parameters of the polished and textured (porous/etched/oxidized) ZrB_2-based composites.

635 **Figures captions**

636 Fig. 1: SEM images of the surface of various ZrB_2-based ceramics showing different microstructural features. a) ZBM0-s
637 by SHS/SPS, b) ZBM20-ps by pressureless sintering; c) ZBM10 by HP and d) porous ZBM10P by pressureless sintering
638 in presence of pore-generating agent. Pores are marked with dotted circles.
639
640 Fig. 2: SEM images of the polished surfaces of hot pressed ZrB_2-based composites with increasing $MoSi_2$ amount: a) 5
641 vol%, b) 20 vol%, c) 30 vol% and d) 50 vol%.
642
643 Fig. 3: a)-b) SEM images of the chemically etched surface of ZBM10 with corresponding EDS spectra in c).
644
645 Fig. 4: a) X-ray diffraction patterns of ZBM10 upon exposure to oxidizing environment at 800°C and 1200°C for 10 hours
646 and corresponding SEM images of the external surface oxidized at b)-d) at 800°C and e)-g) 1200°C. d) and g) are
647 magnified images of the boxed areas in c) and f), respectively.
648
649 Fig. 5: Topographic maps of the ZBM10 sample upon different surface finishing a) as-polished, b) chemically etched
650 (ZBMetc), c) oxidized at 800°C (ZBM800) and d) oxidised at 1200°C (ZBM1200) for 10 hours.
651
652 Fig. 6: a) Comparison of hemispherical reflectance spectra of hot pressed ZrB_2 materials as a function of the additive
653 amount. The spectrum of SiC is also shown for reference. b) Comparison between the two samples with 20% $MoSi_2$ as a
654 function of the processing technique. c) Comparison between the spectra of dense, porous and etched ZBM10. d)
655 Comparison amongst polished and oxidized ZBM10 samples at 800 or 1200°C, together with that of a reference
656 amorphous SiO_2.
657
658 Fig.7: Comparison of the spectral normal emittance of ZBM10 samples and SiC at 1100 K. Due to thermal contact losses
659 at the ceramic pellet/heater interface, 1100K is the maximum temperature actually obtained for these samples. Spectral
660 features at around 2.5, 3, 4 and 6 μm wavelength, which are shown by all samples, are instrumental artifacts due to
661 unbalanced absorption by air gases.
662
663 Fig. 8: a) Solar absorbance, α, and b) Spectral selectivity, α/ε, for the series ZBMX, dense samples.
664

665 Fig. 9: Spectral selectivity, α/ε, and solar absorbance, α, for the pristine and treated samples. Horizontal lines in each plot
666 identify the values obtained for SiC.

Highlights

- Effect of microstructure and finishing on the optical properties of diverse ZrB_2 materials
- Surface texturing by chemical etching led to higher solar absorbance and efficiency
- Oxidation significantly changes the borides properties which behave similar to SiC
- Superior durability and temperature stability enables UHTCs to operate above 500°C
- UHTCs performances in solar absorbers overpass SiC-based materials ones